https://doi.org/10.5194/egusphere-2026-2584
Preprint. Discussion started: 4 June 2026

Two-Dimensional Hydrodynamic Modelling of Glacial Lake Outburst Flood Scenarios from Chubda Tsho: Breach Sensitivity and Downstream Flood Dynamics in the Chamkhar Chhu Basin, Bhutan

Tenzin Namgay[1]*, Kasun De Silva[1,2], Nimal Wijayaratna[1,2], and Lalith Rajapakse[1,2]

[1]UNESCO-Madanjeet Singh Centre for South Asia Water Management (UMCSAWM), Department of Civil Engineering, University of Moratuwa, Moratuwa 10400, Sri Lanka
[2]Department of Civil Engineering, University of Moratuwa, Moratuwa 10400, Sri Lanka

Correspondence to: Tenzin Namgay (tenzinthimphu111@gmail.com)

Abstract. Glacial lake outburst floods (GLOFs) are high-magnitude, short-duration hazards in glacier-fed Himalayan basins, where steep valley confinement can amplify downstream flood intensity. Despite the identification of Chubda Tsho as a potentially dangerous glacial lake in Bhutan, hydrodynamic assessments of potential outburst floods from this lake have not yet been reported. This study evaluates potential GLOF scenarios from Chubda Tsho using inflows generated by a calibrated and independently validated Hydrologic Engineering Center's Hydrologic Modelling System (HEC-HMS), coupled with two-dimensional (2D) simulations in the Hydrologic Engineering Center's River Analysis System (HEC-RAS). The model was calibrated against the July 2007 flood (NSE = 0.90) and validated using the August 2015 event (NSE = 0.56). Hydrodynamic performance was assessed using an extreme-event hydrograph from Cyclone Aila (2009) and compared with observed inundation extent. Results show good agreement, with a Critical Success Index (CSI) of 0.67, a total area difference of 2.56%, and close correspondence between simulated (1.60 km²) and observed (1.56 km²) inundation extents within the 16.14 km² Chamkhar Valley model domain. The Chamkhar Valley contains approximately 8.41 km² of habitable area. Three breach scenarios representing 50%, 75%, and 100% lake-volume release were simulated using empirically derived breach relationships. Flood waves reach the Chamkhar Valley between approximately 1 h 50 min and 2 h 15 min after breach initiation. Peak discharge increases from 2,114 $m^3 s^{-1}$ to 5,258 $m^3 s^{-1}$, accompanied by nonlinear increases in peak depth (8.4–12.8 m) and velocity (5.0–7.6 m s^{-1}). While inundation extent remains constrained by valley geometry, flood depth and velocity increase disproportionately with breach magnitude. Results indicate that downstream hydraulic intensity is strongly influenced by breach magnitude, while warning time remains limited in confined Himalayan valleys. This highlights the value of validated 2D hydrodynamic modelling for GLOF hazard assessment in Himalayan catchments with limited observational data.

Keywords: dam-break analysis; flood routing; inundation mapping; model validation; unsteady flow

https://doi.org/10.5194/egusphere-2026-2584
Preprint. Discussion started: 4 June 2026

1 Introduction

Glacial lake outburst floods (GLOFs) are among the most destructive hydrological hazards in glacier-fed mountain environments, generating high-magnitude flood waves that propagate rapidly downstream following moraine- or ice-dam failure (Carrivick and Tweed, 2016; Westoby et al., 2014). In the Hindu Kush–Himalaya (HKH) region, accelerated glacier retreat and glacial lake expansion under a warming climate have increased concern regarding the frequency and magnitude of potential outburst events (Harrison et al., 2018; Hock et al., 2019; Zhang et al., 2024). Steep valley gradients, confined floodplains, and limited attenuation capacity can amplify downstream flood intensity, making scenario-based hazard assessment essential for risk-informed planning (Huggel et al., 2004; Worni et al., 2014).

Hydrodynamic modelling has become a central tool for GLOF hazard analysis. While one-dimensional (1D) approaches are computationally efficient, they may inadequately represent lateral floodplain processes and depth–velocity interactions in confined mountain valleys (Horritt and Bates, 2002). Two-dimensional (2D) unsteady-flow models provide improved representation of terrain-controlled flow redistribution and channel–floodplain interactions, which are critical for analysing extreme flood propagation in steep basins (Neal et al., 2012; Teng et al., 2017). However, in Himalayan catchments with limited observational data, many hydrodynamic applications remain constrained because simulations are often not independently evaluated against observed extreme inundation extents, reducing confidence in predicted inundation patterns and hydraulic behaviour (Somos-Valenzuela et al., 2016; Westoby et al., 2014).

Bhutan has experienced destructive GLOF events in recent decades, including the 1994 Lugge Tsho outburst (Watanabe and Rothacher, 1996), highlighting the vulnerability of narrow Himalayan valleys to high-energy flood waves. National assessments have identified Chubda Tsho as a potentially dangerous glacial lake within the Chamkhar Chhu Basin (National Center for Hydrology and Meteorology [NCHM], 2019). Although basin-scale hazard evaluations have highlighted downstream exposure (Rinzin et al., 2023; Wangchuk and Tsubaki, 2024), independently evaluated 2D hydrodynamic assessments remain limited in Bhutan and across many Himalayan basins.

This study evaluates downstream flood behaviour associated with potential outburst scenarios from Chubda Tsho in the Chamkhar Chhu Basin. A two-dimensional Hydrologic Engineering Center's River Analysis System (HEC-RAS) model is first assessed using the Cyclone Aila (2009) inundation extent before being applied to three hypothetical breach scenarios representing 50%, 75%, and 100% lake-volume release. The analysis focuses on downstream flood timing and hydraulic intensity, including peak discharge, flood depth, and flow velocity along the Chamkhar Valley corridor. The results provide a validated 2D hydrodynamic framework for assessing GLOF hazard propagation in steep Himalayan river systems with limited observational data.

2 Study Area

The study focuses on potential flood propagation originating from Chubda Tsho, a moraine-dammed glacial lake located in the northern headwaters of the Chamkhar Chhu river system in Bhutan (Figure 1). The lake is situated at approximately

https://doi.org/10.5194/egusphere-2026-2584
Preprint. Discussion started: 4 June 2026

4,868 m a.s.l., with a surface area of about 1.39 km² and an estimated storage volume of 21.69 × 10⁶ m³. It has been classified as a potentially dangerous glacial lake in national assessments (NCHM, 2019), as shown in Figure 1b. The upstream Chamkhar Chhu Basin covers approximately 1,448 km² and spans elevations from about 2,590 m to 6,822 m above sea level, representing a typical high-relief Himalayan catchment (Figure 1a). Meltwater streams from glaciated headwaters converge to form the Chamkhar Chhu River, which flows southward through steep mountain valleys.

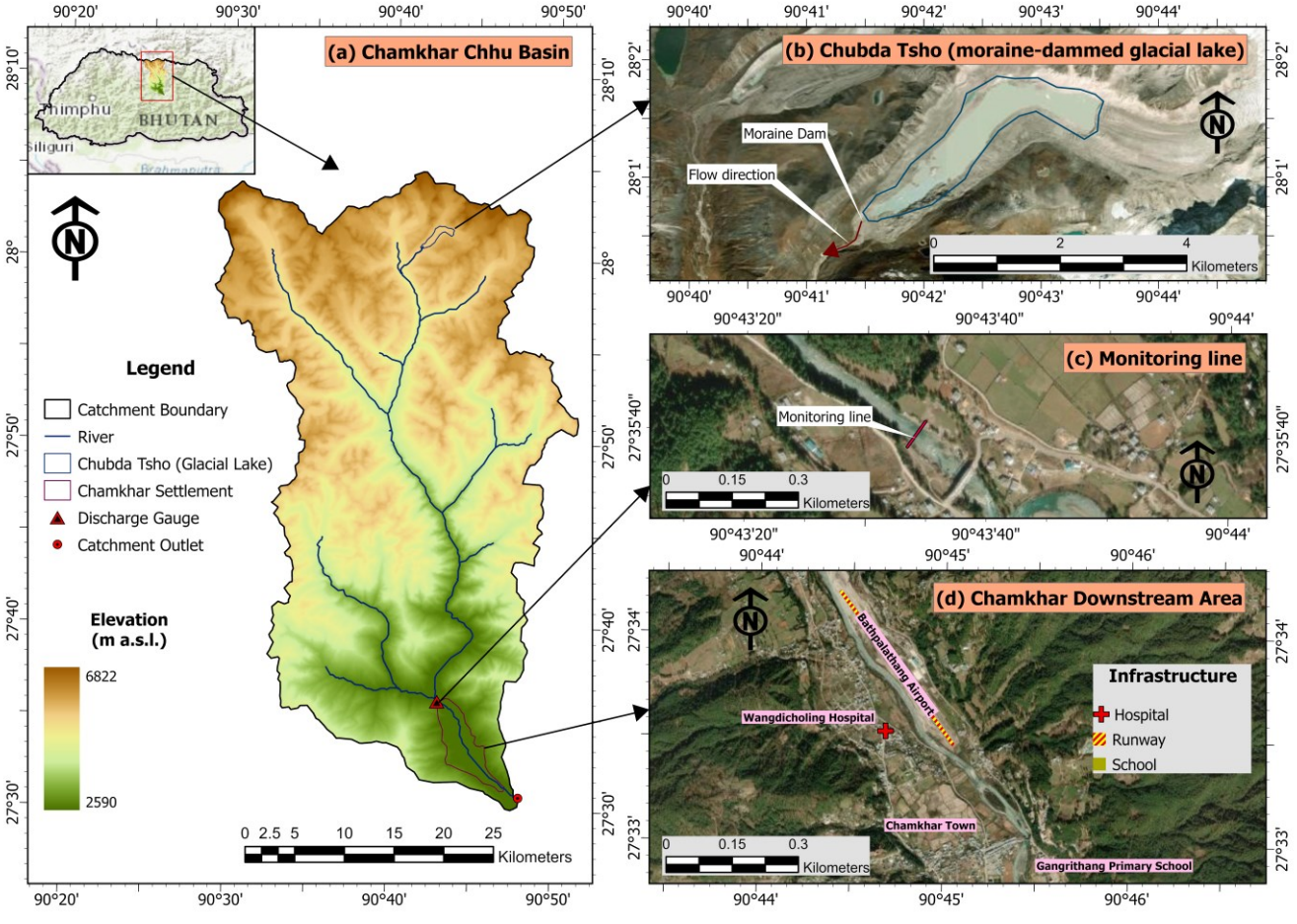

Figure 1: Study area showing (a) the Chamkhar Chhu Basin, (b) Chubda Tsho (moraine-dammed glacial lake), (c) the monitoring line, and (d) the Chamkhar Valley downstream area with key infrastructure (sources: Esri, Vantor, Earthstar Geographics, and the GIS User Community | Powered by Esri).

Downstream of the lake, the river travels approximately 47 km through a confined valley corridor before entering the Chamkhar Valley, where settlements and infrastructure are concentrated along a relatively narrow valley floor (Figure 1d). The Chamkhar Valley contains approximately 8.41 km² of habitable area, derived from land-use classification. This downstream reach defines the 2D hydrodynamic modelling domain used to simulate flood propagation under potential GLOF

https://doi.org/10.5194/egusphere-2026-2584
Preprint. Discussion started: 4 June 2026

scenarios. Hydraulic outputs used for downstream analysis were extracted from a monitoring line (Figure 1c) at the upstream entry to the Chamkhar Valley, representing the transition between the upstream mountain corridor and the downstream valley reach. The monitoring line was defined in the HEC-RAS geometry using two endpoints at (E 275575 m, N 3054358 m) and (E 275541 m, N 3054307 m) in Universal Transverse Mercator (UTM) Zone 46N (WGS 84).

3 Methods

A coupled hydrological–hydrodynamic modelling framework was used to simulate potential GLOF scenarios originating from Chubda Tsho and to analyse downstream flood behaviour in the Chamkhar Valley. The workflow integrates rainfall–runoff modelling using the Hydrologic Engineering Center's Hydrologic Modelling System (HEC-HMS), hydrodynamic flood simulation using HEC-RAS 2D, and scenario-based generation of dam breach hydrographs. A schematic overview of the modelling framework is presented in Figure 2.

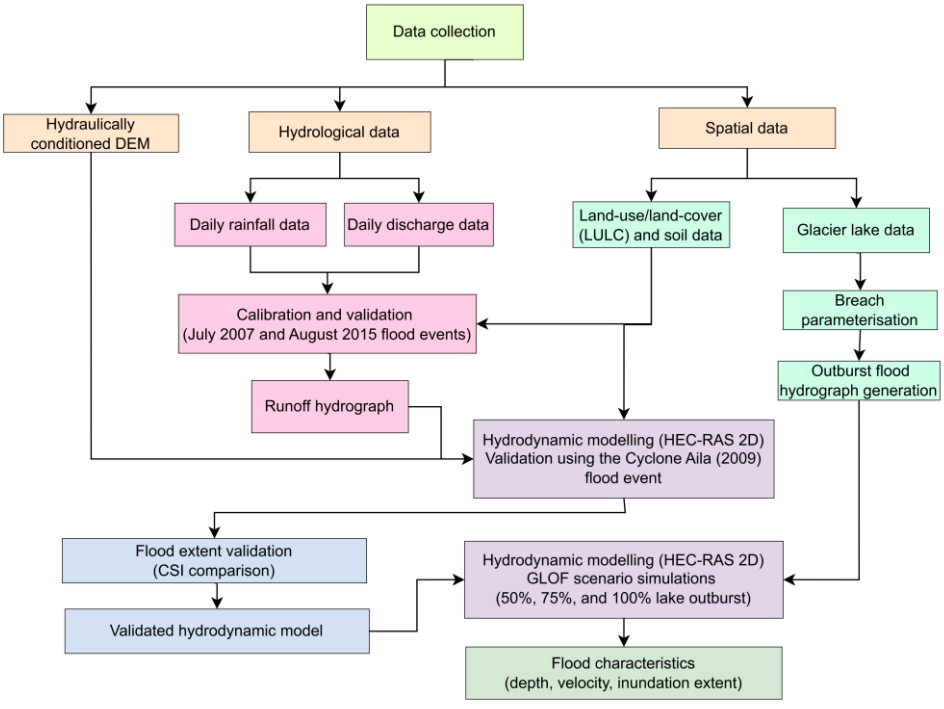

Figure 2: Workflow of the coupled hydrological–hydrodynamic modelling framework used for model validation and GLOF simulation.

3.1 Hydrological Modelling Framework

Event-based rainfall–runoff modelling was performed using HEC-HMS (U.S. Army Corps of Engineers, 2023a) to generate inflow hydrographs for hydrodynamic model validation. The Chamkhar Chhu Basin was represented as a single hydrological

https://doi.org/10.5194/egusphere-2026-2584
Preprint. Discussion started: 4 June 2026

unit draining to the downstream gauging station. The model was calibrated using the July 2007 flood event and validated using the August 2015 event without parameter modification. Model performance was evaluated using the Nash–Sutcliffe efficiency (NSE) and percent bias (PBIAS) statistics. The calibrated model was subsequently used to simulate runoff generated by the Cyclone Aila (2009) extreme rainfall event, which provided the upstream boundary condition for hydrodynamic model evaluation.

3.2 Two-Dimensional Hydrodynamic Modelling Framework

Flood-wave propagation downstream of Chubda Tsho was simulated using the two-dimensional unsteady-flow module of HEC-RAS (U.S. Army Corps of Engineers, 2023b). The hydrodynamic model was set up to simulate flood-wave routing along the Chamkhar Valley reach downstream of Chubda Tsho, where settlements and critical infrastructure are concentrated along a relatively narrow valley floor. The extreme rainfall-driven flood associated with Cyclone Aila (2009) was used to test whether the HEC-RAS 2D setup reproduces flood-wave propagation and inundation patterns under high-discharge conditions.

The validated setup was then applied to scenario-based GLOF simulations representing varying breach magnitudes. Model setup included terrain preparation, computational mesh generation, hydraulic parameter assignment, boundary condition specification, and unsteady flow simulation. Breach parameters and scenario-specific outburst hydrographs were derived using empirical relationships, and model outputs (flood depth, velocity, and inundation extent) were used to assess downstream flood behaviour.

3.2.1 Breach Parameterisation

The physical characteristics of Chubda Tsho required for breach parameter estimation and outburst hydrograph generation were obtained from national glacial lake inventory assessments (NCHM, 2019). Key parameters include lake surface area, storage volume, and maximum depth, which together control the magnitude and temporal evolution of potential outburst hydrographs. The parameters used for the breach analysis are summarised in Table 1.

Table 1. Physical characteristics of Chubda Tsho used for breach parameter estimation.

Parameter	Value	Unit
Lake Area	1.39	km^2
Lake Volume	21.69×10^6	m^3
Maximum Depth	56.00	m

To represent a range of physically plausible failure magnitudes, three hypothetical GLOF scenarios were defined corresponding to the release of 50%, 75%, and 100% of the total lake storage volume. For each scenario, the released water volume and breach depth were scaled proportionally from the maximum lake depth (Table 2). These scenarios represent plausible magnitudes of moraine-dam breaches rather than deterministic predictions of failure.

https://doi.org/10.5194/egusphere-2026-2584
Preprint. Discussion started: 4 June 2026

Table 2. Definition of hypothetical GLOF scenarios based on percentage lake-volume release.

Scenario	Released volume (%)	Outburst volume (m³)	Breach depth (m)
Partial outburst	50	10.85×10^6	28
Moderate outburst	75	16.27×10^6	42
Full outburst	100	21.69×10^6	56

Breach parameters were estimated using the empirical relationships proposed by Froehlich (1995, 2008), which relate breach geometry and peak discharge to reservoir volume and dam height. These relationships have been widely applied in dam-break and GLOF studies in data-scarce mountainous environments. The average breach width was estimated as:

$$B_{ave} = 0.1803 K_o {V_w}^{0.32} {h_b}^{0.32} \quad (1)$$

where B_{ave} is the average breach width (m), V_w is the released water volume (m³), h_b is the breach depth (m), K_o is a failure-mode coefficient. A value of $K_o = 1$ was adopted to represent a non-overtopping, erosion-driven breach mechanism.

Breach formation time was represented as:

$$t_f = 0.00254 {V_w}^{0.53} {h_b}^{-0.90} \quad (2)$$

where t_f is the breach formation time (s).

Peak breach discharge was estimated as:

$$Q_p = 0.607 {V_w}^{0.295} {h_b}^{1.24} \quad (3)$$

where Q_p is the peak outflow discharge (m³ s⁻¹).

The breach bottom width was calculated as:

$$B_{bw} = B_{ave} - (h_b \times S_s) \quad (4)$$

where B_{bw} is the breach bottom width (m) and S_s is the breach side-slope ratio. A constant side slope of 0.9H:1V (horizontal: vertical) was assumed for all scenarios. Because the B_{bw} is calculated from B_{ave} and h_b under a constant side-slope assumption, it does not necessarily increase monotonically with breach magnitude. The resulting breach parameters for the three outburst scenarios are summarised in Table 3. Peak discharge values represent the empirical breach-outflow estimated at the Chubda Tsho dam site using the relationships proposed by Froehlich (1995, 2008).

Table 3. Estimated breach parameters derived using Froehlich's empirical relationships.

Scenario (%)	B_{ave} (m)	t_f (hr)	B_{bw} (m)	Q_p (m³ s⁻¹)
50	60.6	0.68	35.40	4,498
75	74.5	0.58	36.68	8,382
100	86.3	0.52	35.85	13,035

https://doi.org/10.5194/egusphere-2026-2584
Preprint. Discussion started: 4 June 2026

3.2.2 Hydrograph Construction

Synthetic outburst hydrographs were constructed assuming a single-peak breach process, with peak discharge occurring near the midpoint of breach development.

The time to peak discharge was defined as:

$$t_p = 0.5 \times t_f \tag{5}$$

The total hydrograph duration was approximated as:

$$t_{total} = 3 \times t_p \tag{6}$$

The rising limb of the hydrograph was represented using a linear relationship:

$$Q(t) = Q_p \frac{t}{t_p} \qquad 0 \le t \le tp \tag{7}$$

while the recession limb was represented using an exponential decay function:

$$Q(t) = Q_p e^{-(t-t_p)/k} \qquad t > tp \tag{8}$$

where k is a recession constant controlling hydrograph decay. The value of k was determined iteratively to ensure mass conservation, such that the integrated hydrograph volume equals the specified outburst volume:

$$V_w = \int_0^{t_{end}} Q(t)dt \tag{9}$$

Minor adjustments to the recession constant (≤2.3%) were applied to match the intended released volumes while preserving the characteristic sharp rising limb and gradual recession typical of GLOF hydrographs. The final peak discharge values used in the synthetic hydrographs (Table 4) therefore differ slightly from the empirical breach peak discharge estimates derived using Froehlich's relationships (Table 3), because the recession constant was adjusted during hydrograph construction to satisfy volume conservation.

Table 4. Characteristics of synthetic GLOF hydrographs used as upstream boundary conditions.

Scenario (%)	Final peak discharge ($m^3 s^{-1}$)	t_p (hr)	k (hr)	Hydrograph volume (m^3)	t_{total} (hr)
50	4,412	0.35	0.52	10.85×10^6	2.05
75	8,189	0.28	0.41	16.27×10^6	1.75
100	12,782	0.27	0.34	21.69×10^6	1.57

https://doi.org/10.5194/egusphere-2026-2584
Preprint. Discussion started: 4 June 2026

The resulting hydrographs for the three breach scenarios are shown in Figure 3.

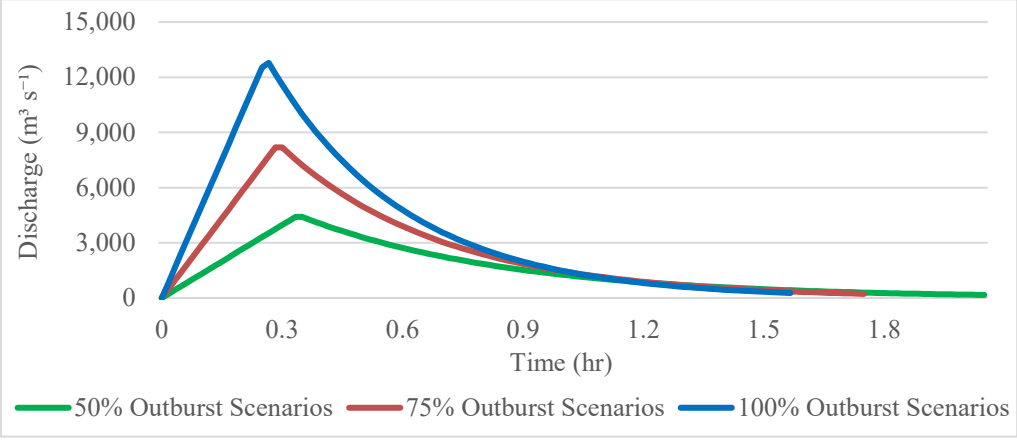

Figure 3: Synthetic GLOF hydrographs for the 50%, 75%, and 100% scenarios used as upstream boundary conditions.

3.2.3 Hydrodynamic Model Setup

The hydrodynamic model domain was constructed using a conditioned digital elevation model (DEM) derived from ALOS PALSAR data and projected to Universal Transverse Mercator (UTM Zone 46N, WGS 84). The terrain dataset used in this study was corrected through vertical bias adjustment and channel refinement to improve hydraulic connectivity and reduce artificial flow discontinuities, following standard terrain-conditioning procedures. The 2D flow area was delineated along the Chamkhar Chhu river corridor, extending from the Chubda Tsho outlet to the downstream Chamkhar Valley, where settlements and infrastructure are concentrated.

The final 2D computational domain covered 16.14 km², focusing on the flood-prone valley floor and settled areas while excluding steep surrounding terrain unlikely to experience direct inundation. Hydraulic outputs for downstream flood analysis were extracted at a monitoring line (Figure 1c) located at the upstream entry to the Chamkhar Valley. The monitoring line was defined in the HEC-RAS geometry using two endpoints at (E 275575 m, N 3054358 m) and (E 275541 m, N 3054307 m). This monitoring line is located approximately 47 km downstream of Chubda Tsho and represents the transition point where the river enters the downstream Chamkhar Valley reach. The monitoring line was used consistently to extract flood hydrographs, peak discharge, arrival time, flow velocity, and flood depth for all simulated scenarios.

The computational domain was discretised using a structured 2D mesh consisting of approximately 224,000 cells, with an average face length of 13 m and a mean cell area of 171 m². Breaklines were applied along riverbanks to preserve channel alignment and prevent unrealistic lateral flow spreading across steep valley margins. Local mesh refinement with a grid spacing of 5 m × 5 m was implemented in downstream areas containing dense settlements and critical infrastructure to improve the resolution of flood depth and velocity. Spatially distributed Manning's roughness coefficients (n) were assigned based on 2020 land-use and land-cover (LULC) data following standard hydraulic references (Chow, 1959; Westoby et al., 2014). Roughness

https://doi.org/10.5194/egusphere-2026-2584
Preprint. Discussion started: 4 June 2026

values were applied to represent river channels, vegetated floodplains, agricultural areas, and built-up surfaces within the computational domain. The assigned Manning's n values are summarised in Table 5.

Table 5. Manning's roughness coefficients assigned to LULC classes in the hydrodynamic model.

LULC Class	Manning's *n*	LULC Class	Manning's *n*
Alpine Scrubs	0.050	Shrubs	0.050
Built-up	0.040	Snow and Glacier Cover	0.010
Agricultural Land	0.035	Water Bodies	0.010
Forests	0.150	River channel	0.050
Meadows	0.150	Landslides	0.060
Moraines	0.030	Sandy	0.030
Rocky Outcrops	0.030	Non-built-up	0.050

Note: Manning's *n* values adapted from Cenderelli and Wohl (2001); Chow (1959); Rickenmann (1999); Somos-Valenzuela et al. (2016); Westoby et al. (2014).

The spatial distribution of roughness coefficients used in the hydrodynamic model is illustrated in Figure 4, which shows the detailed downstream model area.

Figure 4: Spatial distribution of Manning's roughness coefficients (n) derived from LULC and soil data.

Surface infiltration was simulated in the 2D domain using the SCS Curve Number method with spatially distributed parameters derived from land-cover and soil datasets. Given that flood routing is dominated by the channel wave during high-discharge conditions, infiltration is expected to have a secondary influence on simulated depth and velocity. Upstream boundary conditions for model validation were defined using the hydrograph generated from the Cyclone Aila rainfall–runoff simulation (Figure 7). For GLOF simulations, synthetic breach hydrographs were applied as upstream inflow conditions (Figure 3).

https://doi.org/10.5194/egusphere-2026-2584
Preprint. Discussion started: 4 June 2026

The downstream boundary condition was specified using a normal-depth approach based on the longitudinal channel slope of 0.025 derived from the model geometry. Before the scenario simulations, the computational domain was pre-wetted using a short warm-up run with a steady inflow of 5 $m^3 s^{-1}$ to establish initial hydraulic conditions within the channel. The resulting hydraulic state was stored as a restart file and used as the initial condition for all GLOF simulations.

All simulations were performed using the unsteady-flow solver in HEC-RAS based on the full shallow-water equations (SWE-ELM), with adaptive time stepping governed by the Courant stability condition to ensure numerical stability and accurate representation of flood-wave dynamics. The adaptive scheme allows automatic adjustment of the computational time step in response to local flow conditions, particularly within refined grid regions. Output intervals were selected to adequately capture hydrograph evolution, inundation extent, depth, and velocity with sufficient temporal resolution. All simulations were run for 4 h to capture flood arrival, peak passage, and initial attenuation within the downstream Chamkhar Valley reach.

Model outputs were processed using RAS Mapper and exported for spatial analysis and flood hazard mapping. Model geometry and hydraulic parameters were kept constant across simulations to ensure that differences in results reflect only variations in breach scenarios.

3.2.4 Hydrodynamic Model Validation Approach

To evaluate the reliability of the hydrodynamic model for simulating extreme flood propagation, the model was assessed using the flood event associated with Cyclone Aila (2009). The discharge hydrograph generated from the calibrated hydrological model was applied as the upstream boundary condition in the HEC-RAS 2D model, while the downstream boundary condition was defined using the normal-depth approach. Observed inundation extent data for the Cyclone Aila event were available as a georeferenced image derived from satellite observations.

The inundated area was manually digitised within a GIS environment to generate a polygon representing the observed inundation footprint. This polygon was used as the reference dataset for validating the simulated inundation extent produced by the hydrodynamic model. Two complementary validation approaches were applied. First, qualitative validation was performed through visual comparison of the simulated and observed inundation extents to assess whether the model reproduced the spatial pattern of flooding along the river corridor and adjacent flood-prone areas. Second, quantitative validation was conducted using spatial overlay analysis to measure the agreement between observed and simulated inundation polygons.

Model performance was evaluated using the Critical Success Index (CSI), which quantifies the spatial overlap between simulated and observed inundation extents (Horritt and Bates, 2002). The CSI is defined as:

$$CSI = \frac{A_{overlap}}{A_{observed} + A_{simulated} - A_{overlap}} \quad (10)$$

where $A_{overlap}$ represents the area where both simulated and observed inundation overlap, $A_{observed}$ is the observed inundated area, and $A_{simulated}$ is the simulated inundation area.

https://doi.org/10.5194/egusphere-2026-2584
Preprint. Discussion started: 4 June 2026

The spatial comparison metrics derived from this analysis were used to evaluate the ability of the hydrodynamic model to reproduce extreme flood behaviour prior to applying the model to the synthetic GLOF scenarios.

4 Results

4.1 Hydrological Model Calibration and Validation

The July 2007 flood event was used for model calibration, while the August 2015 event served as the validation. During calibration, the observed peak discharge was 263 $m^3 s^{-1}$ and the simulated peak was 258 $m^3 s^{-1}$ (Figure 5), yielding NSE = 0.90 and PBIAS = −6.0%. For the validation event, the observed peak discharge reached 283 $m^3 s^{-1}$, while the simulated peak was 219 $m^3 s^{-1}$ (Figure 6), with NSE = 0.56 and PBIAS = −3.2%.

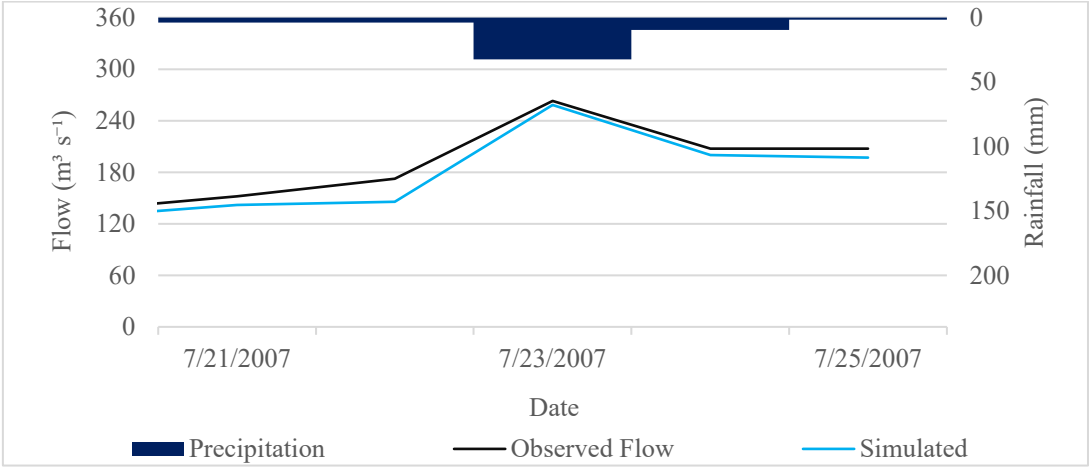

Figure 5: Comparison of observed and simulated discharge for the July 2007 calibration event.

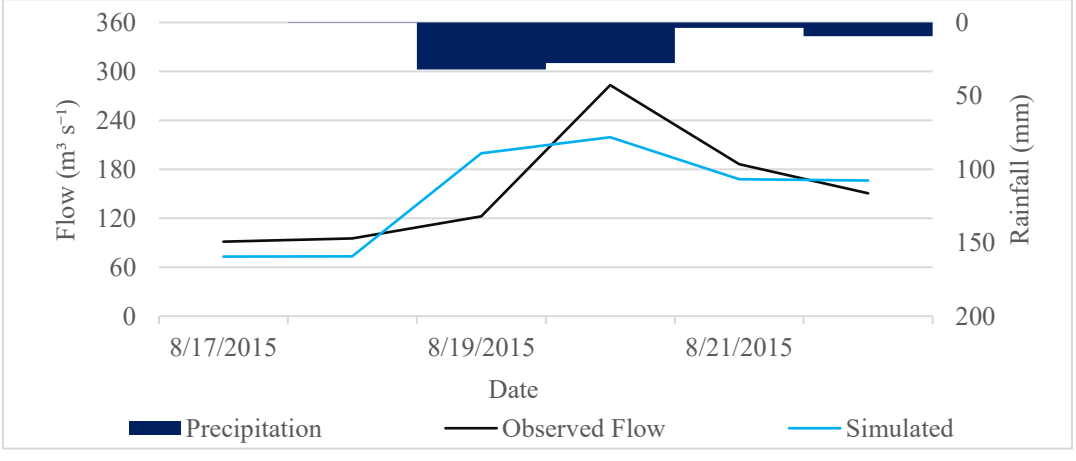

Figure 6: Comparison of observed and simulated discharge for the August 2015 validation event.

https://doi.org/10.5194/egusphere-2026-2584
Preprint. Discussion started: 4 June 2026

Peak discharge values and performance metrics for the calibration and validation events are summarised in Table 6.

Table 6. Observed and simulated peak discharge and performance metrics for calibration and validation events.

Event	Type	Observed Peak ($m^3 s^{-1}$)	Simulated Peak ($m^3 s^{-1}$)	PBIAS (%)	NSE
July 2007	Calibration	263	258	-6.0	0.90
August 2015	Validation	283	219	-3.2	0.56

4.2 Hydrodynamic Model Validation

Following hydrological model calibration and validation, the model was applied to simulate runoff generated by the extreme rainfall event associated with Cyclone Aila (2009). The observed peak discharge for this event was 586 $m^3 s^{-1}$, while the simulated peak was 553 $m^3 s^{-1}$. The resulting hydrograph used as the upstream boundary condition for hydrodynamic validation is shown in Figure 7.

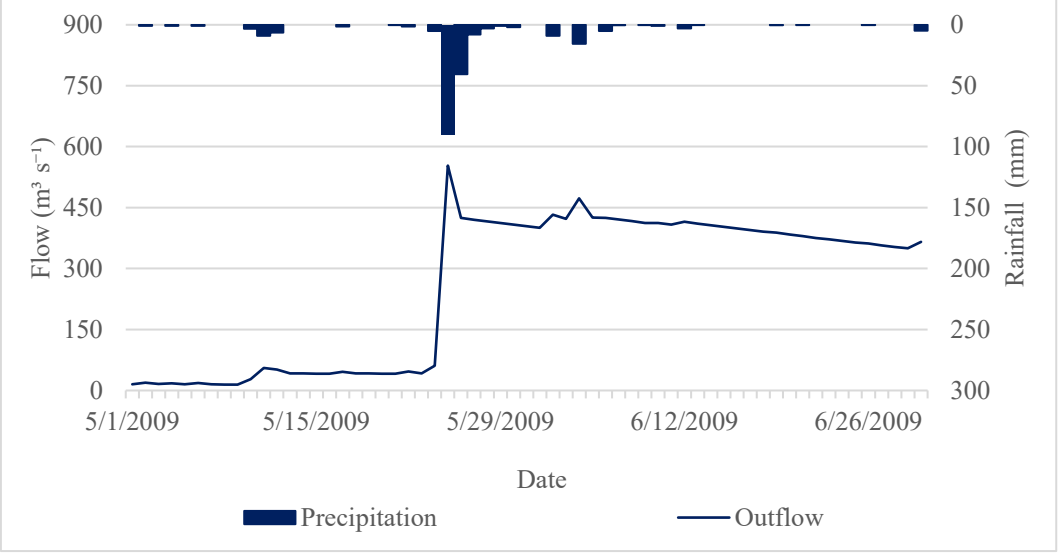

Figure 7: Simulated runoff hydrograph for the Cyclone Aila (2009) event used as the upstream boundary condition.

Comparison of simulated and observed inundation extents for the Cyclone Aila flood event indicates good hydrodynamic model performance. Within the 16.14 km^2 downstream computational domain, the observed inundation area was 1.56 km^2, while the simulated inundation extent reached 1.60 km^2. The inundation is confined to a narrow valley-aligned corridor along the river channel, where exposed infrastructure is distributed linearly rather than over a continuous area; consequently, features such as the airport runway, bridges, hospital access routes, and parts of Chamkhar Town can be affected within a relatively small inundated area. Spatial overlay analysis shows that 1.27 km^2 of the inundated area was correctly reproduced by the model.

https://doi.org/10.5194/egusphere-2026-2584
Preprint. Discussion started: 4 June 2026

The observed-only inundation area accounted for 0.29 km², whereas the simulated-only inundation covered 0.33 km². The overall difference between observed and simulated inundation extents is 2.56%. Model performance was quantified using the Critical Success Index (CSI), which yielded a value of 0.67 (Table 7). This indicates good spatial agreement between simulated and observed inundation under extreme discharge conditions, as CSI values exceeding 0.6 are commonly considered satisfactory in flood-inundation modelling (Horritt and Bates, 2002; Neal et al., 2012).

Table 7. Comparison of observed and simulated inundation extents and associated spatial metrics for the Cyclone Aila (2009) event.

Parameter	Area (km²)
Observed Inundation Area	1.56
Simulated Inundation Area	1.60
Overlapping Inundation Area	1.27
Observed-only Inundation Area	0.29
Simulated-only Inundation Area	0.33
Percent Difference (%)	2.56
Critical Success Index (CSI)	0.67

The confusion matrix (Figure 8) shows that the model correctly predicted both flooded and non-flooded areas across most of the 16.14 km² computational domain.

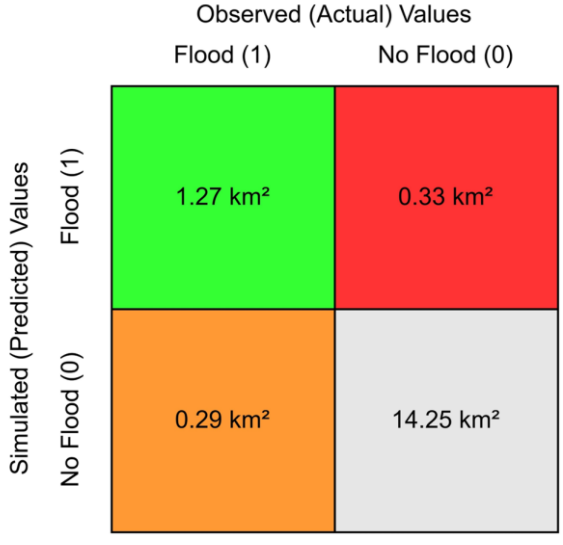

Figure 8: Confusion matrix showing agreement between observed and simulated inundation extents for the Cyclone Aila (2009) event.

https://doi.org/10.5194/egusphere-2026-2584
Preprint. Discussion started: 4 June 2026

Visual comparison further confirms that the model reproduces the primary flood corridor along the Chamkhar Chhu. The spatial agreement between the observed and simulated inundation patterns is shown in Figure 9, with only minor variations along shallow floodplain margins.

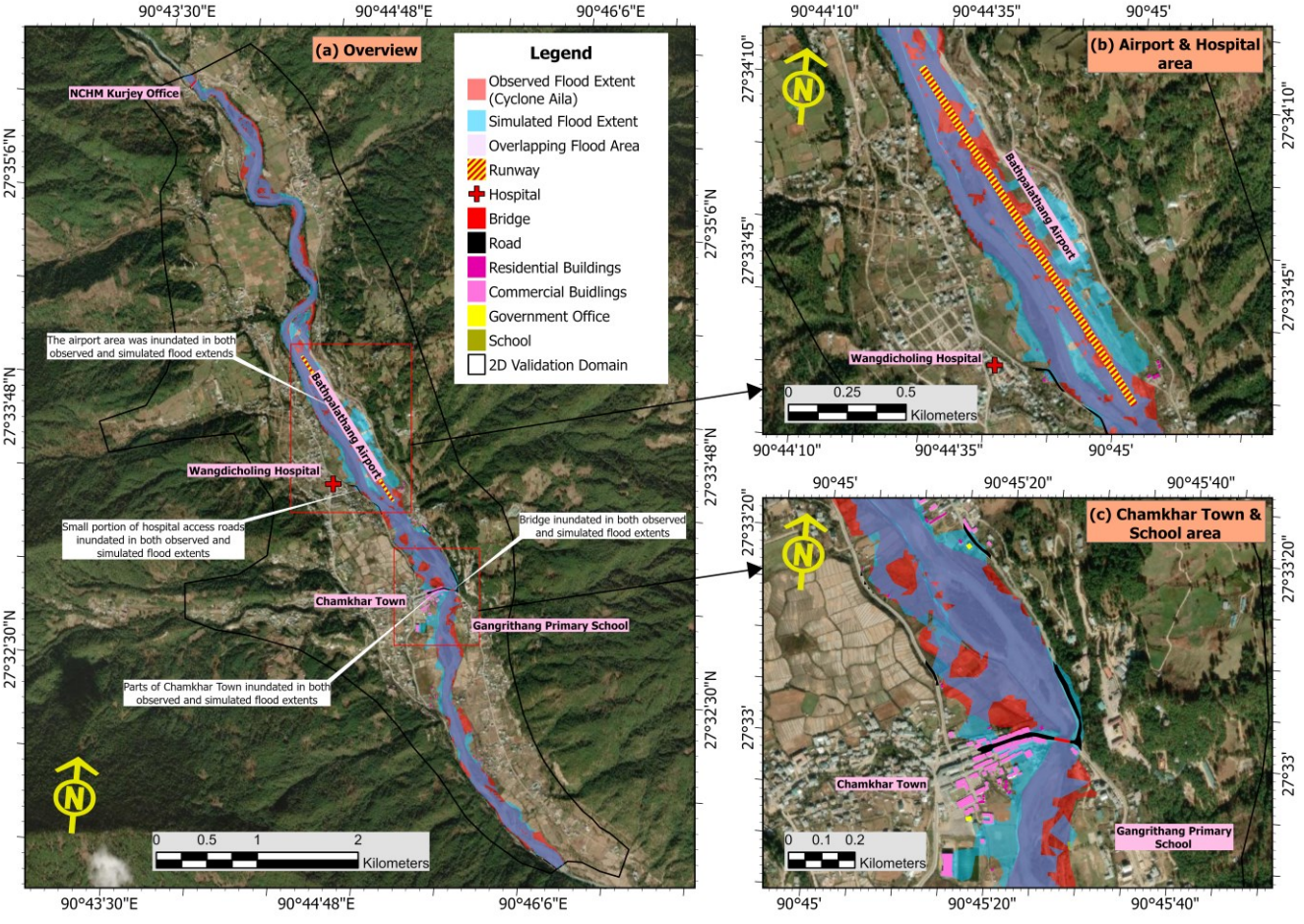

Figure 9: Spatial comparison of observed and simulated inundation extents for the Cyclone Aila (2009) event within the downstream Chamkhar Valley (sources: Esri, Vantor, Earthstar Geographics, and the GIS User Community | Powered by Esri).

4.3 Downstream Flood Response under GLOF Scenarios

Three hypothetical GLOF scenarios were simulated corresponding to the release of 50%, 75%, and 100% of the Chubda Tsho lake volume. Simulated flood waves reached the monitoring location at the upstream entry to the Chamkhar Valley between 1 h 50 min and 2 h 15 min after breach initiation (Table 8).

https://doi.org/10.5194/egusphere-2026-2584
Preprint. Discussion started: 4 June 2026

Peak discharge, depth, and velocity increase with breach magnitude (Table 8), while values at the downstream monitoring location remain lower than the estimated peak breach outflow at the lake outlet (Table 3) due to flood-wave attenuation and temporary storage along the ~47 km river corridor.

Table 8. Downstream hydraulic parameters at the monitoring location for different GLOF scenarios.

Parameter	Outburst Volume Scenario		
	50%	75%	100%
Peak discharge ($m^3 s^{-1}$)	2,114	3,715	5,258
Arrival time (hh:mm)	2:15	1:55	1:50
Time to peak (hh:mm)	2:25	2:05	2:00
Total volume ($10^6 m^3$)	7.4	12.2	16.3
Peak velocity ($m s^{-1}$)	5.0	6.4	7.6
Peak depth (m)	8.4	10.9	12.8

Percentage changes between scenarios show that increases in discharge, depth, and velocity are not proportional to breach magnitude. Between the 50% and 100% scenarios, peak discharge increased by approximately 149%, while peak velocity and peak depth increased by about 52%, indicating a nonlinear increase in hydraulic intensity with breach magnitude.

Temporal variations in discharge, stage elevation, velocity, and depth at the downstream monitoring location are shown in Figure 10–Figure 12.

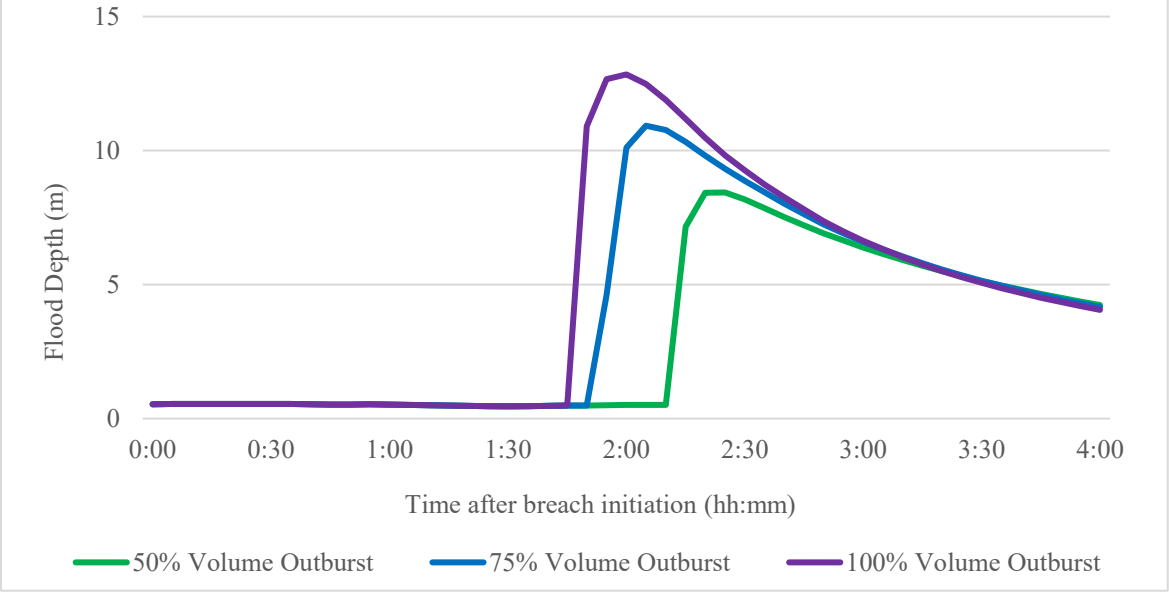

Figure 10: Temporal variation of flood depth at the downstream monitoring location under 50%, 75%, and 100% GLOF scenarios.

https://doi.org/10.5194/egusphere-2026-2584
Preprint. Discussion started: 4 June 2026

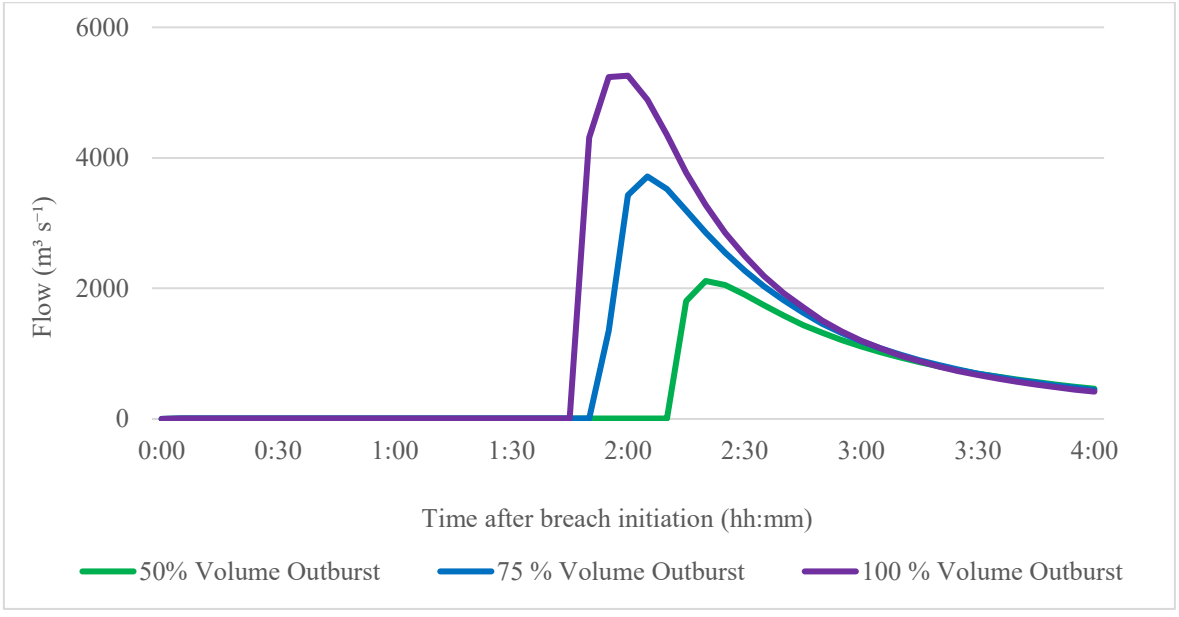

Figure 11: Simulated discharge hydrographs at the downstream monitoring location for the 50%, 75%, and 100% GLOF scenarios.

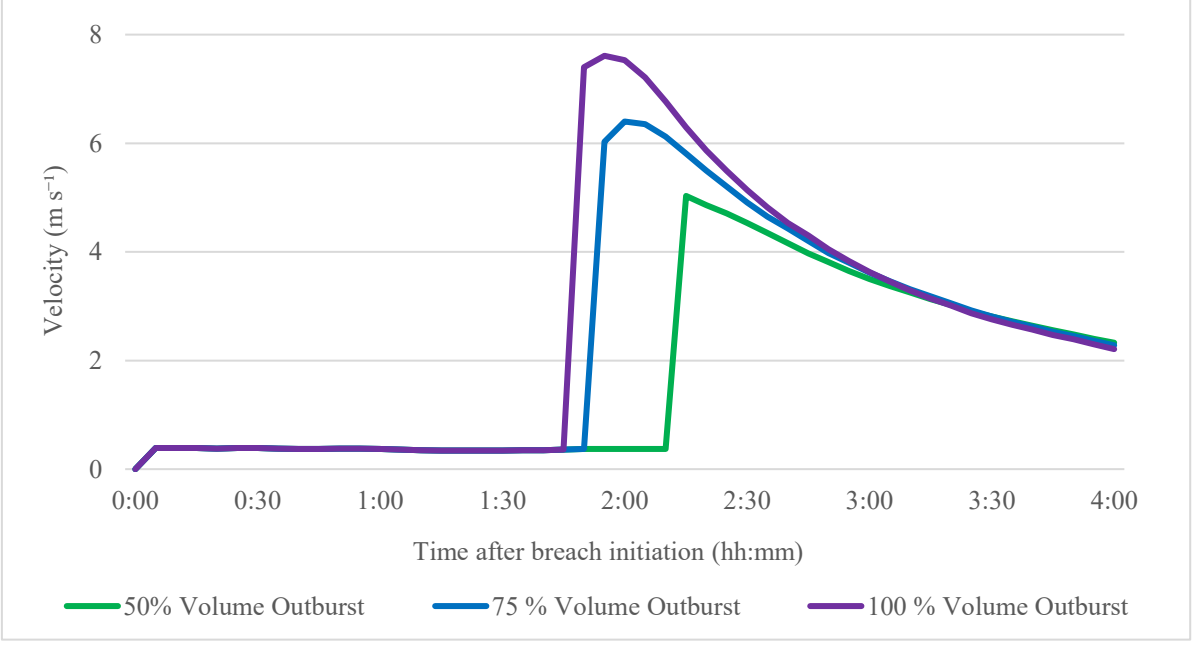

Figure 12: Temporal variation of flow velocity at the downstream monitoring location for the 50%, 75%, and 100% GLOF scenarios.

https://doi.org/10.5194/egusphere-2026-2584
Preprint. Discussion started: 4 June 2026

4.4 Downstream Hazard Characteristics

Spatial distributions of flood depth for the three scenarios are shown in Figure 13. Under the 50% breach scenario, inundation remains largely confined to the river channel and immediate margins. In the 75% scenario, areas affected by depths exceeding 1 m expand along the river corridor and into adjacent low-lying floodplain areas. The 100% breach scenario produces widespread channel inundation, with depths exceeding 2 m along extended sections of the valley corridor.

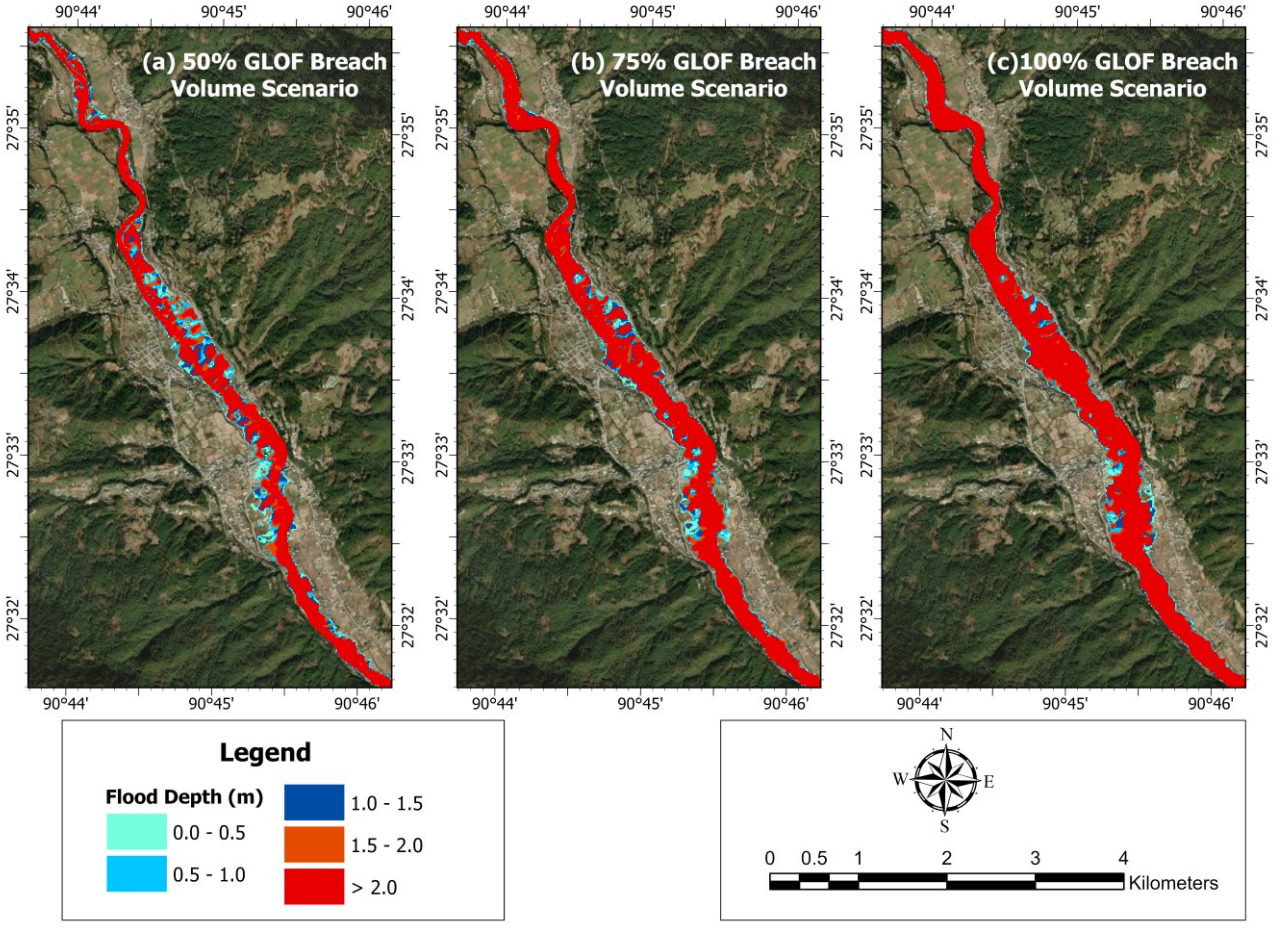

Figure 13: Spatial distribution of flood depth in the downstream reach for the 50%, 75%, and 100% GLOF scenarios (sources: Esri, Vantor, Earthstar Geographics, and the GIS User Community | Powered by Esri).

https://doi.org/10.5194/egusphere-2026-2584
Preprint. Discussion started: 4 June 2026

290 Flood velocity patterns increase with breach magnitude, particularly in confined valley sections and near channel constrictions, as illustrated in Figure 14. At the downstream monitoring location, water depths remain between 4.0 and 4.2 m at 4 h after flood arrival, with only minor differences among scenarios.

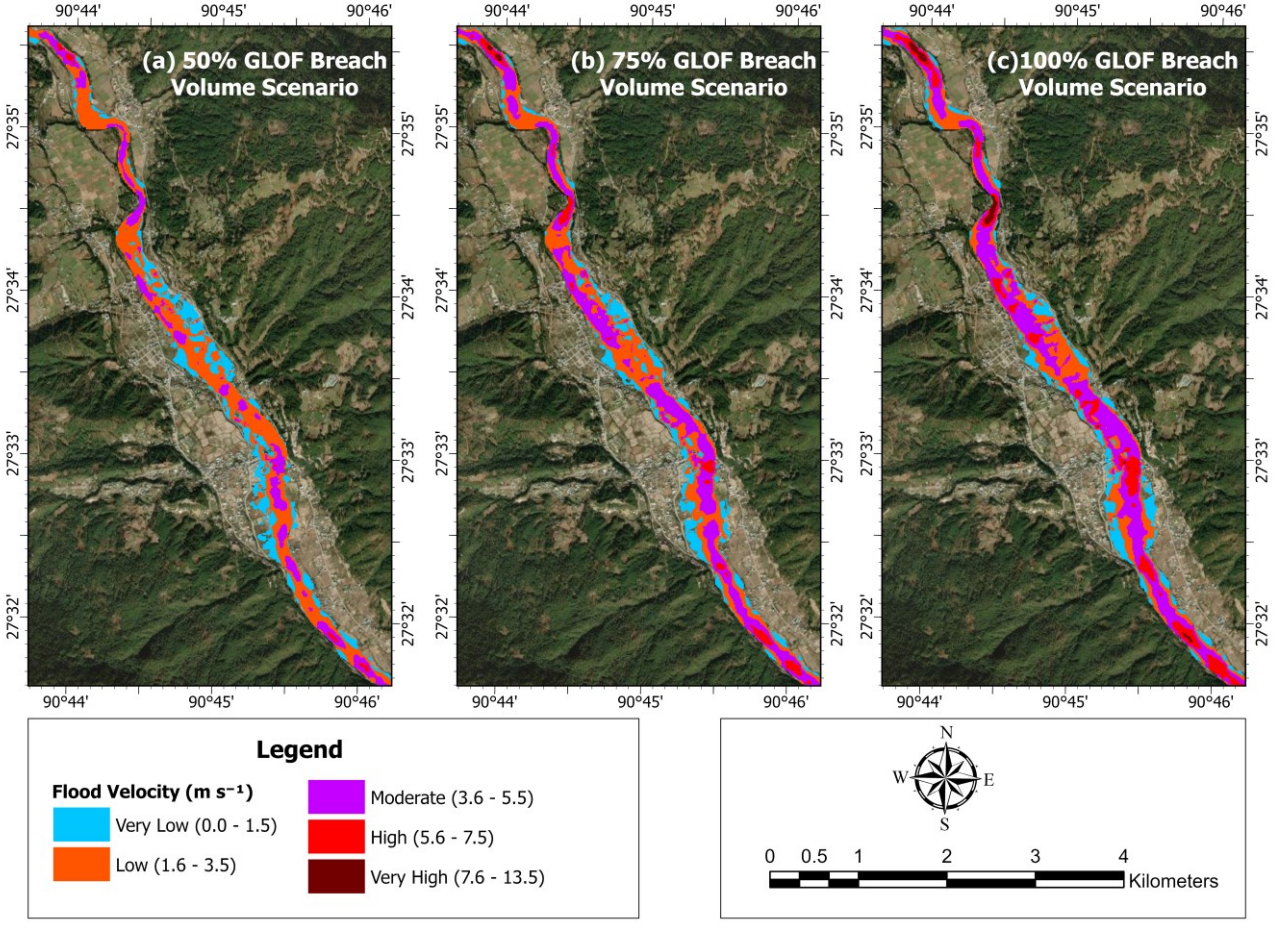

Figure 14: Spatial distribution of flow velocity in the downstream reach for the 50%, 75%, and 100% GLOF scenarios (sources: Esri, 295 Vantor, Earthstar Geographics, and the GIS User Community | Powered by Esri).

5 Discussion

5.1 Hydrological Model Performance

The HEC-HMS hydrological modelling was used primarily to generate the extreme-event hydrograph for hydrodynamic modelling. Calibration against the July 2007 flood event showed strong agreement (NSE = 0.90; Figure 5), while validation 300 using the August 2015 event produced acceptable performance (NSE = 0.56; Figure 6).

https://doi.org/10.5194/egusphere-2026-2584
Preprint. Discussion started: 4 June 2026

The calibrated HEC-HMS model also reproduced the peak discharge associated with the Cyclone Aila event with reasonable agreement (observed 586 $m^3 s^{-1}$; simulated 553 $m^3 s^{-1}$). The resulting hydrograph (Figure 7) therefore provides a reasonable upstream boundary condition for simulating the flood using the HEC-RAS 2D hydrodynamic model, which was subsequently used to simulate the flood due to the synthetic GLOF breach scenarios.

5.2 Hydrodynamic Model Validation

The spatial comparison between simulated and observed inundation extents indicates that the model reliably captures downstream flooding behaviour, as reflected by the obtained CSI value (Table 7). This CSI value falls within the range generally considered satisfactory for flood-inundation modelling, particularly where validation relies on remotely sensed inundation extents (Horritt and Bates, 2002; Neal et al., 2012). Minor discrepancies occur mainly along shallow floodplain margins and valley edges, as evident in Figure 9, and likely reflect uncertainties in the observed flood boundary derived from satellite imagery rather than deficiencies in the hydrodynamic model structure. Overall, these results support the reliability of the hydrodynamic model for simulating flood routing within the Chamkhar Valley reach.

5.3 Controls on Downstream Flood Dynamics

The breach scenario simulations demonstrate a nonlinear increase in hydraulic intensity with increasing breach magnitude, as shown by the downstream hydrographs and peak hydraulic variables in Table **8** and Figure 10–Figure 12. Larger breach volumes produce substantial increases in peak discharge, flood depth, and flow velocity, consistent with the high-energy characteristics of GLOF events in steep Himalayan river systems. This amplification reflects the rapid translation of increased inflow into flow energy under steep-gradient, confinement-controlled conditions, where limited lateral storage restricts attenuation of peak discharge. Although the estimated breach outflow at the lake outlet exceeds 13,000 $m^3 s^{-1}$ (Table 3), the peak discharge simulated at Chamkhar Valley is substantially lower due to flood-wave attenuation and temporary storage along the ~47 km confined valley reach.

The simulated hydrographs indicate that warning times for downstream communities and critical infrastructure are limited, reinforcing the importance of rapid detection and communication in the Chamkhar Valley. Despite substantial increases in peak discharge, the lateral extent of inundation remains relatively limited across scenarios, as shown in the flood-depth distributions (Figure 13). The narrow valley geometry confines floodwaters primarily within the main river corridor and adjacent floodplain, with the strongest hydraulic intensification occurring in confined valley sections (Figure 13 and Figure 14). In steep mountain valleys, flood depth and flow velocity provide more meaningful indicators of hazard intensity than inundation area alone. Smaller outbursts may still cause prolonged disruption through sustained inundation, whereas larger outbursts pose a greater immediate life-threatening risk due to extreme depth and velocity.

https://doi.org/10.5194/egusphere-2026-2584
Preprint. Discussion started: 4 June 2026

5.4 Limitations and Future Work

Uncertainty in the simulated GLOF hazards arises primarily from empirical breach parameterisation, hydrological input variability, and terrain representation. Breach parameters and outburst hydrographs were derived using the empirical relationships proposed by Froehlich (1995, 2008), which were originally developed for earthen embankment dams. Applying these formulations to moraine-dammed glacial lakes introduces uncertainty in breach geometry, formation time, and peak discharge. Consequently, the simulated 50–100% lake-release cases should be interpreted as plausible scenario envelopes rather than deterministic predictions of failure magnitude.

Hydrodynamic validation relied on the extreme rainfall-driven flood associated with Cyclone Aila (2009), in the absence of documented historical GLOF observations for the study basin. While this event provides a practical benchmark for testing flood routing and inundation behaviour under high-discharge conditions, it does not directly validate moraine-breach processes or sediment-laden GLOF flow behaviour. Future work should explore probabilistic breach modelling, improved representation of melt processes, and additional independent flood observations to further strengthen GLOF hazard assessment in Himalayan catchments.

6 Conclusion

This study applied a coupled hydrological–hydrodynamic framework to evaluate potential GLOF hazards originating from Chubda Tsho in the Chamkhar Chhu Basin, Bhutan. The framework was used to generate upstream inflow conditions and simulate downstream flood propagation under scenario-based breach conditions.

Independent validation using the extreme rainfall-driven Cyclone Aila (2009) flood event demonstrated that the hydrodynamic model reproduces observed inundation patterns with good spatial agreement (CSI = 0.67) and a total inundation-area difference of 2.56%. These results indicate that the modelling system can reliably represent flood routing and inundation behaviour under high-discharge conditions in the Chamkhar Valley.

Scenario-based simulations representing 50%, 75%, and 100% release of the Chubda Tsho lake volume show rapid downstream flood propagation. Flood waves travel quickly through the upstream mountain corridor, reaching the Chamkhar Valley in approximately 1 h 50 min to 2 h 15 min after breach initiation. Increasing breach magnitude produces a nonlinear amplification of hydraulic intensity, with peak discharge increasing from 2,114 to 5,258 $m^3 s^{-1}$, accompanied by substantial increases in flood depth and flow velocity.

Despite these increases in discharge magnitude, the steep topographic gradient and narrow valley geometry constrain lateral flood expansion and concentrate hydraulic energy within the main river corridor. As a result, flood depth and velocity emerge as more informative indicators of hazard intensity than inundation area alone in confined Himalayan valleys.

https://doi.org/10.5194/egusphere-2026-2584
Preprint. Discussion started: 4 June 2026

The results indicate that a validated 2D hydrodynamic modelling approach provides physically consistent estimates of downstream GLOF hazards in steep, Himalayan catchments with limited observational data. The rapid downstream propagation of simulated flood waves highlights the need for real-time glacial lake monitoring, automated early-warning systems, and rapid communication to support evacuation and disaster preparedness in glacier-fed Himalayan environments.

Code and data availability

Hydrological and hydrodynamic simulations were conducted using HEC-HMS (v4.9) and HEC-RAS (v6.6) developed by the U.S. Army Corps of Engineers. Terrain data were derived from the SRTM DEM (90 m; USGS) and ALOS PALSAR DEM (12.5 m; Alaska Satellite Facility). Land-use/land-cover data (2020) were obtained from the Bhutan National Spatial Data Infrastructure (NSDI), and soil classification data were obtained from the National Soil Services Center, Bhutan, which were used to derive hydrological parameters. Information on glacial lake characteristics was obtained from the NCHM (2019) glacial lake inventory.

Hydrometeorological observations (rainfall, discharge) and observed inundation extent data were provided by the NCHM, Bhutan, and are subject to institutional data-sharing restrictions. Derived model inputs and simulation outputs supporting the findings of this study are available from the corresponding author upon reasonable request, subject to approval by the data-providing institutions.

Author contributions

Tenzin Namgay designed the study, performed modelling, and prepared the manuscript. Kasun De Silva, Nimal Wijayaratna, and Lalith Rajapakse supervised the research and contributed to manuscript revision.

Competing interests

The authors declare that they have no conflict of interest.

Acknowledgements

The authors gratefully acknowledge the support of the UNESCO Madanjeet Singh Centre for South Asia Water Management (UMCSAWM), University of Moratuwa, Sri Lanka, for providing the academic and research environment for this study. The authors also thank the supervisors for their guidance and constructive feedback throughout the research. The National Center for Hydrology and Meteorology (NCHM), Bhutan, and other national agencies are acknowledged for providing hydrometeorological and geospatial datasets essential for this work.

https://doi.org/10.5194/egusphere-2026-2584
Preprint. Discussion started: 4 June 2026

Financial support

This research was supported by the South Asia Foundation (SAF) through a scholarship awarded by the UNESCO-Madanjeet Singh Centre for South Asia Water Management (UMCSAWM).

References

Carrivick, J. L. and Tweed, F. S.: A global assessment of the societal impacts of glacier outburst floods, Global Planet. Change, 144, 1–16, https://doi.org/10.1016/j.gloplacha.2016.07.001, 2016.

Cenderelli, D. A. and Wohl, E. E.: Peak discharge estimates of glacial-lake outburst floods and "normal" climatic floods in the Mount Everest region, Nepal, Geomorphology, 40, 57–90, https://doi.org/10.1016/S0169-555X(01)00037-X, 2001.

Chow, V. T.: Open-channel hydraulics, McGraw-Hill, 1959.

Froehlich, D. C.: Embankment dam breach parameters revisited, in: Proceedings of the 1995 ASCE Water Resources Engineering Conference, 887–891, American Society of Civil Engineers, 1995.

Froehlich, D. C.: Embankment dam breach parameters and their uncertainties, J. Hydraul. Eng., 134, 1708–1721, https://doi.org/10.1061/(ASCE)0733-9429(2008)134:12(1708), 2008.

Harrison, S., Kargel, J. S., Huggel, C., Reynolds, J. M., Shugar, D. H., Betts, R. A., Emmer, A., Glasser, N., Haritashya, U. K., Klimeš, J., Reinhardt, L., Schaub, Y., Wiltshire, A., Regmi, D., and Vilímek, V.: Climate change and the global pattern of moraine-dammed glacial lake outburst floods, The Cryosphere, 12, 1195–1209, https://doi.org/10.5194/tc-12-1195-2018, 2018.

Hock, R., Rasul, G., Adler, C., Cáceres, B., Gruber, S., Hirabayashi, Y., Jackson, M., Kääb, A., Kang, S., Kutuzov, S., Milner, A., Molau, U., Morin, S., Orlove, B., and Steltzer, H.: High mountain areas, in: IPCC Special Report on the Ocean and Cryosphere in a Changing Climate, edited by: Pörtner, H.-O., Roberts, D. C., Masson-Delmotte, V., Zhai, P., Tignor, M., Poloczanska, E., Mintenbeck, K., Alegría, A., Nicolai, M., Okem, A., Petzold, J., Rama, B., and Weyer, N. M., IPCC, 131–202, https://www.ipcc.ch/site/assets/uploads/sites/3/2019/11/06_SROCC_Ch02_FINAL.pdf, 2019.

Horritt, M. S. and Bates, P. D.: Evaluation of 1D and 2D numerical models for predicting river flood inundation, J. Hydrol., 268, 87–99, https://doi.org/10.1016/S0022-1694(02)00121-X, 2002.

Huggel, C., Haeberli, W., Kääb, A., Bieri, D., and Richardson, S.: An assessment procedure for glacial hazards in the Swiss Alps, Can. Geotech. J., 41, 853–864, https://doi.org/10.1139/t04-053, 2004.

National Center for Hydrology and Meteorology (NCHM): Reassessment of potentially dangerous glacial lakes in Bhutan, Royal Government of Bhutan, https://www.nchm.gov.bt/attachment/ckfinder/userfiles/files/Re-assessment%20of%20Potentailly%20Dangerous%20Glacial%20Lakes.pdf (last access: 8 May 2026), 2019.

Neal, J., Schumann, G., and Bates, P.: A subgrid channel model for simulating river hydraulics and floodplain inundation over large and data sparse areas, Water Resour. Res., 48, W11521, https://doi.org/10.1029/2012WR012514, 2012.

https://doi.org/10.5194/egusphere-2026-2584
Preprint. Discussion started: 4 June 2026

Rickenmann, D.: Empirical relationships for debris flows, Nat. Hazards, 19, 47–77, https://doi.org/10.1023/A:1008064220727, 1999.

Rinzin, S., Zhang, G., Sattar, A., Wangchuk, S., Allen, S. K., Dunning, S., and Peng, M.: GLOF hazard, exposure, vulnerability, and risk assessment of potentially dangerous glacial lakes in the Bhutan Himalaya, J. Hydrol., 619, 129311, https://doi.org/10.1016/j.jhydrol.2023.129311, 2023.

Somos-Valenzuela, M. A., Chisolm, R. E., Rivas, D. S., Portocarrero, C., and McKinney, D. C.: Modelling a glacial lake outburst flood process chain: The case of Lake Palcacocha and Huaraz, Peru, Hydrol. Earth Syst. Sci., 20, 2519–2543, https://doi.org/10.5194/hess-20-2519-2016, 2016.

Teng, J., Jakeman, A. J., Vaze, J., Croke, B. F. W., Dutta, D., and Kim, S.: Flood inundation modelling: A review of methods, recent advances and uncertainty analysis, Environ. Model. Softw., 90, 201–216, https://doi.org/10.1016/j.envsoft.2017.01.006, 2017.

U.S. Army Corps of Engineers: HEC-HMS hydrologic modelling system technical reference manual, Hydrologic Engineering Center, 2023a.

U.S. Army Corps of Engineers: HEC-RAS river analysis system hydraulic reference manual, Hydrologic Engineering Center, 2023b.

Wangchuk, T. and Tsubaki, R.: A glacial lake outburst flood risk assessment for the Phochhu River Basin, Bhutan, Nat. Hazards Earth Syst. Sci., 24, 2523–2540, https://doi.org/10.5194/nhess-24-2523-2024, 2024.

Watanabe, T. and Rothacher, D.: The 1994 Lugge Tsho glacial lake outburst flood, Bhutan Himalaya, Mt. Res. Dev., 16, 77–81, https://doi.org/10.2307/3673897, 1996.

Westoby, M. J., Glasser, N. F., Brasington, J., Hambrey, M. J., Quincey, D. J., and Reynolds, J. M.: Modelling outburst floods from moraine-dammed glacial lakes, Earth-Sci. Rev., 134, 137–159, https://doi.org/10.1016/j.earscirev.2014.03.009, 2014.

Worni, R., Huggel, C., Clague, J. J., Schaub, Y., and Stoffel, M.: Coupling glacial lake impact, dam breach, and flood processes: A modelling perspective, Geomorphology, 224, 161–176, https://doi.org/10.1016/j.geomorph.2014.06.031, 2014.

Zhang, G., Carrivick, J. L., Emmer, A., Shugar, D. H., Veh, G., Wang, X., Labedz, C., Mergili, M., Mölg, N., Huss, M., Allen, S., Sugiyama, S., and Lützow, N.: Characteristics and changes of glacial lakes and outburst floods, Nat. Rev. Earth Environ., 5, 447–462, https://doi.org/10.1038/s43017-024-00554-w, 2024.